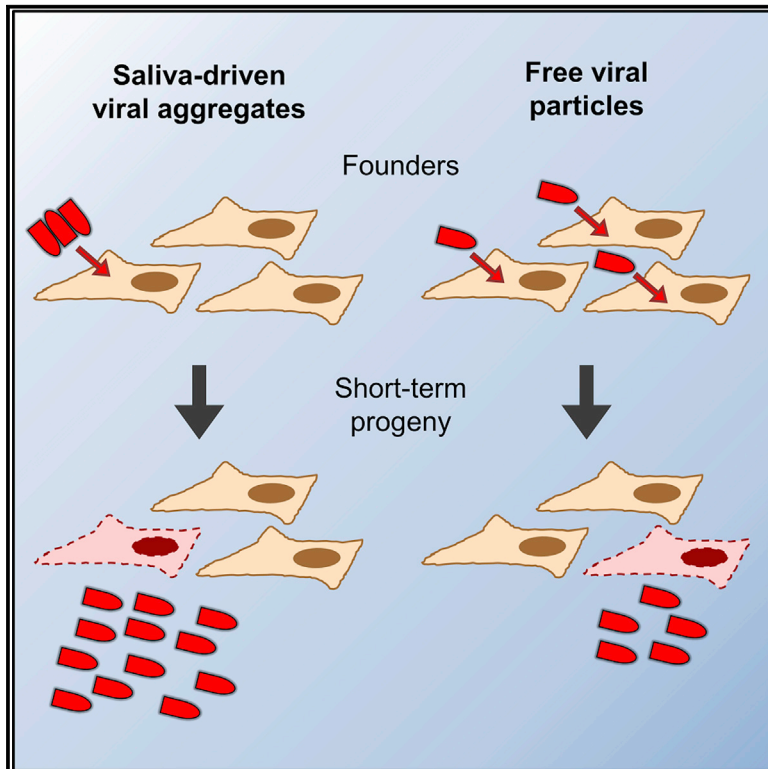# Collective Infection of Cells by Viral Aggregates Promotes Early Viral Proliferation and Reveals a Cellular-Level Allee Effect

Graphical Abstract

Authors
Iván Andreu-Moreno, Rafael Sanjuán

Correspondence
rafael.sanjuan@uv.es

In Brief
Some viruses can infect cells in the form of multi-virion structures called collective infectious units. Andreu-Moreno and Sanjuán show that collective infection by aggregates of vesicular stomatitis virus accelerates viral progeny production and increases short-term fitness compared to free viruses, revealing a cellular-level Allee effect.

Highlights

- Saliva-driven virion aggregation tends to increase short-term viral fitness

- Infecting cells with multiple virions accelerates the per virus release of progeny

- The fitness effect of aggregation depends on cellular permissivity to infection

- The benefits of aggregation correlate with the strength of cellular innate immunity

CellPress

Collective Infection of Cells by Viral Aggregates Promotes Early Viral Proliferation and Reveals a Cellular-Level Allee Effect

Iván Andreu-Moreno[1] and Rafael Sanjuán[1,2,*]
[1]Institute for Integrative Systems Biology (I2SysBio), Universitat de València, C/Catedrático Agustín Escardino 9, Paterna, València 46980, Spain
[2]Lead Contact
*Correspondence: rafael.sanjuan@uv.es
https://doi.org/10.1016/j.cub.2018.08.028

SUMMARY

In addition to the conventional release of free, individual virions, virus dispersal can involve multi-virion assemblies that collectively infect cells. However, the implications of collective infection for viral fitness remain largely unexplored. Using vesicular stomatitis virus, here, we compare the fitness of free versus saliva-aggregated viral particles. We find that aggregation has a positive effect on early progeny production, conferring a fitness advantage relative to equal numbers of free particles in most cell types. The advantage of aggregation resides, at least partially, in increasing the cellular multiplicity of infection. In mouse embryonic fibroblasts, the per capita, short-term viral progeny production peaked for a dose of ca. three infectious particles per cell. This reveals an Allee effect restricting early viral proliferation at the cellular level, which should select for dispersal in groups. We find that genetic complementation between deleterious mutants is probably not the mechanism underlying the fitness advantage of collective infection. Instead, this advantage is cell type dependent and correlates with cellular permissivity to the virus, as well as with the ability of host cells to mount an antiviral innate immune response.

INTRODUCTION

In contrast to the traditional view that viruses propagate among cells as individual virions, recent work has described viral spread in groups [1, 2]. For instance, in vesicular stomatitis virus (VSV) [3] and poliovirus [4], virion aggregates can infect cells collectively. In enteroviruses, lipid vesicles containing multiple virions are released from infected cells before lysis and serve as intercellular vehicles for viral spread [5]. Similarly, multiple marseillevirus particles are jointly wrapped in large extracellular vesicles derived from the amoebal endoplasmic reticulum [6]. In baculoviruses, inter-host transmission takes place in the form of pools of virions encased in a protein matrix, called occlusion bodies [7]. Use of cell-cell contacts for the delivery of large number of viral particles

has also been shown in many viruses. For instance, human T cell leukemia virions accumulate in extracellular matrix components called "viral biofilms," which are used for cell-cell virion transfer [8]. Other viruses, including HIV-1, measles virus, vaccinia virus, and herpes virus, subvert existing cell-cell contacts or induce new ones, using cells as vehicles for the joint transfer of multiple particles [9, 10]. In fecal-oral-transmitted viruses, such as poliovirus, gut bacteria act as attractors of viral particles, also promoting their joint spread [11]. Finally, inter-host transmission in a cell-associated manner is also possible but remains understudied, except for HIV-1, where it has been shown to be an important transmission route [12].

Despite evidence for these various modes of collective spread in viruses, little is known about their implications for viral fitness. All else being equal, multi-virion propagules should be disfavored because they reduce dispersal capacity and, hence, the efficiency of intra-host spread and inter-host transmission. To illustrate this, consider infected cells (or hosts) producing N groups each containing S particles. The infection will reach, at most, N cells (hosts) in the next viral generation, whereas an equal amount of non-aggregated progeny would reach NS cells (hosts). Therefore, for collective spread to be selectively advantageous, there should be benefits offsetting this cost, yet these benefits remain unclear. Specifically, spread in groups will increase viral fitness if the average progeny yield of such groups exceeds NS, which means that cellular resources should be exploited more efficiently compared to individual virions. Dispersal in groups can be advantageous if invasion of new spots (here, cells) is subject to an Allee effect, defined as a positive relationship between fitness and population size or density. The Allee effect is believed to be an important factor-limiting population establishment because it slows down proliferation or even leads to extinction of small founder populations [13]. Allee effects have been documented in many animal and plant species, including invasive and/or parasitic species [14], such as, for instance, entomopathogenic nematodes [15]. Interestingly, the Allee effect has been demonstrated recently in *Vibrio* bacteria [16]. However, there is no previous evidence for Allee effects in viruses.

One way to examine the fitness effects of dispersal in groups is to compare equal numbers of viral particles in monodisperse versus aggregated form. VSV offers an excellent system to achieve this goal, because virions can be aggregated experimentally [3]. Here, we show that VSV aggregates produce progeny more rapidly than equal numbers of non-aggregated viral
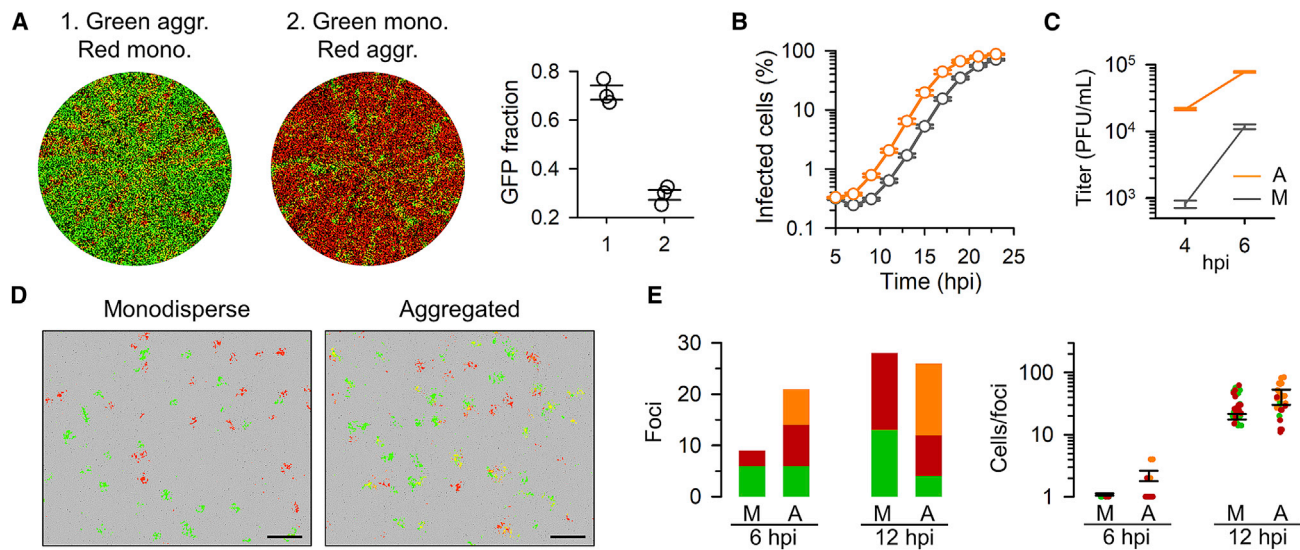
Figure 1. Aggregation Increases Viral Fitness by Promoting Early Growth in MEFs

(A) Whole-well fluorescence microscopy of MEFs inoculated with aggregated VSV-GFP and monodisperse VSV-mCherry particles (1) and with monodisperse VSV-GFP and aggregated VSV-mCherry particles (2). Images were taken at 24 hpi and correspond to one of the three replicate assays performed. The fraction of total fluorescent area occupied by GFP-positive cells is shown in the right graph for the three replicates. Error bars represent SEM.

(B) Growth curve of VSV in MEFs obtained by real-time whole-well fluorescence microscopy. The percentage of fluorescent cells in the well is shown. Grey, monodisperse inoculum; orange, aggregated inoculum. Each data point is the average of three replicates. Error bars represent SEM.

(C) Viral titers in cultures inoculated with aggregates (A) versus monodisperse (M) particles (inoculum: 5,000 PFUs). Three replicates were performed. Error bars represent SEM.

(D) Foci produced in MEFs inoculated with equal numbers of monodisperse versus aggregated particles (14 hpi). VSV-GFP and VSV-mCherry were mixed prior to aggregation. Cells expressing both VSV-GFP and VSV-mCherry appear in yellow. The cell monolayer is shown in phase contrast. The scale bars represent 1 mm.

(E) Analysis of individual infection foci at different time points in MEFs inoculated with monodisperse or aggregated particles. Left: bars indicate the number of foci positive for GFP (green), mCherry (red), or both (orange). Right: number of cells within infection foci (same color legend). Notice that foci containing both VSV-Cherry and VSV-GFP tend to be bigger than those containing a single type. Error bars represent SEM.

See Figure S1 for results obtained in BHK-21 cells.

particles during the first cellular infection cycle and that this confers a competitive advantage to populations founded by aggregates compared to those founded by monodisperse particles. By measuring viral progeny production in cells inoculated with different doses of the virus, we show that the advantage of aggregation may reside in increasing the number of founder particles per cell. Specifically, we found that the per capita progeny production depends on the multiplicity of infection (MOI) in a manner consistent with an Allee effect at the cellular level. The fitness advantage of aggregation is cell type dependent and correlates with cellular permissivity to infection. We suggest that invading cells with multiple viral particles reduces the risk of early stochastic loss and/or provides the virus a head start relative to innate immune responses, increasing the chances of establishing a successful infection locally.

RESULTS

Aggregation of Founder Particles Increases Viral Fitness in MEFs

In previous work, we showed that VSV particles aggregate in the presence of saliva from some donors [3]. To test how initiating the infection with such aggregates determines viral fitness, we competed two recombinant viruses encoding different fluorescent reporters (GFP versus mCherry). For this, we aggregated VSV-GFP with human saliva and kept VSV-mCherry untreated

(i.e., monodisperse) and then mixed the two viruses at a 1:1 particle ratio (as determined by titration before aggregation) and inoculated mouse embryonic fibroblasts (MEFs) at low initial viral density. The infection progressed until invading the entire cell culture at approximately 24 hr post inoculation (hpi). At this time point, 71.3% ± 3.0% of the total fluorescent area corresponded to GFP, as determined by whole-well fluorescence microscopy. In contrast, when we competed monodisperse VSV-GFP against aggregated VSV-mCherry, GFP accounted for only 29.3% ± 2.0% of total fluorescence at 24 hpi (t test: p < 0.001; Figure 1A). Therefore, for an equal input of viral particles, initiating the infection in an aggregated manner increased viral fitness in competition assays. Real-time fluorescence microscopy revealed that the growth curves of viral populations founded by aggregates were left shifted compared to those founded by monodisperse particles, with estimated half-times of 16.7 ± 0.2 hr and 19.1 ± 0.1 hr, respectively (Figure 1B). To confirm this short-term advantage, we titrated supernatants by the plaque assay at time points within or at the boundary of the first infection cycle (4 and 6 hpi). The 4 hpi titer in cells inoculated with monodisperse particles was below the inoculum size, hence showing no evidence of progeny production (eclipse phase). In contrast, aggregates produced a 27-fold higher titer at this time point, exceeding 10^4 plaque-forming units (PFUs) per mL (t test: p < 0.001; Figure 1C). At 6 hpi, cells inoculated with aggregates still produced 6.5 times more progeny (t test: p < 0.001).
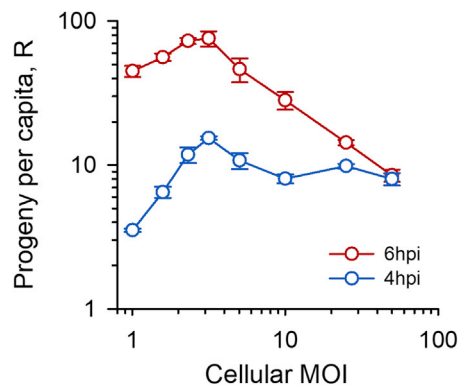
Figure 2. Early Viral Progeny Production Exhibits a Demographic Allee Effect

Per-capita progeny production (R, defined as final-to-initial ratiotiter) in MEFs for different cellular MOI values (defined as the average number of initial PFUs per infected cell). Each data point is the average of three replicates. Error bars represent SEM. See Figure S2 for results obtained in BHK-21 cells.

Therefore, viral aggregation accelerated viral proliferation during the first infection cycle, providing a fitness advantage relative to non-aggregated founders.

Aggregation Does Not Reduce Dispersal Capacity in MEFs

In principle, because each aggregate contains multiple particles, aggregation should reduce the number of infectious units and, hence, reduce dispersal capacity, as argued above. To test whether aggregates infected fewer cells than an equal number of monodisperse particles, we co-incubated VSV-GFP and VSV-mCherry in saliva and counted the number of infection foci produced in MEFs, compared with the foci produced by this same mix without the saliva treatment. A large fraction of the foci produced by saliva-treated viruses were positive for both GFP and mCherry, confirming that aggregates deliver multiple viral genomes to target cells [3] (Figure 1D). Despite this, we did not observe a reduction in the number of foci in cells inoculated with the saliva-aggregated virus compared to those inoculated with untreated viruses. We explored this further by counting infected cells at early time points in an entire well using a minimal VSV-GFP/VSV-Cherry inoculum to ensure sufficient separation of infection foci. At 6 hpi, monodisperse particles produced only 9 individual infected cells, whereas aggregates produced 21 foci of 1.4 ± 0.2 cells on average, infecting 30 total cells (Figure 1E). At 12 hpi, we found similar numbers of foci in cultures infected with monodisperse and aggregated particles (28 and 26, respectively), and foci were slightly, but not significantly, larger in the latter (31.5 ± 2.8 and 38.7 ± 4.0 cells, respectively; t test: p = 0.232). Therefore, aggregation increased the per-particle probability of successfully initiating infection, as determined by the production of infection foci.

The Per-Capita Viral Progeny Production Exhibits an Allee Effect at the Cellular Level

We speculated that viral aggregation was advantageous because it increased the cellular MOI (cMOI) (in PFUs/cell units), defined as the average number of particles that initiate the infec-

tion of a cell. However, other processes were in principle possible, such as, for instance, more efficient cell binding and/or entry of aggregates compared to individual viral particles. To analyze how the cMOI determined progeny production, we inoculated MEFs with doses of monodisperse particles at densities ranging from $D = 0.01$ to $D = 50$ PFU/cell. The cMOI was calculated based on a Poisson model as follows: $cMOI = D/[1 - P(0)]$, where $P(0) = e^{-D}$ is the Poisson distribution null class (notice that cMOI $\geq$ 1). We determined viral titers at 4–6 hpi to obtain the per-capita progeny production during the first cell infection cycle, defined as the final-to-input titer ratio (R). In the absence of an Allee effect, R should decrease with the cMOI as a result of competition for limited resources or remain constant if cellular resources were not limiting. In contrast, at 4 hpi, R was always higher for cMOI > 1 than for cMOI = 1; that is, it always paid off for the virus to invade cells with multiple particles, and R peaked at approximately cMOI = 3 (Figure 2). For instance, doubling the cMOI from 1.58 to 3.16 increased the titer at 4 hpi by seven-fold. At 6 hpi, R peaked at a similar cMOI value but then dropped, probably because of cellular resource exhaustion. At this time point, it still paid off for the virus to invade N cells with S particles each rather than NS cells with one particle each, provided that S $\leq$ 5 PFU/cell. These data show that a demographic Allee effect operates at the cellular level, supporting the possibility that the fitness advantage of aggregation resides at least partially in the collective infection of cells.

The Fitness Benefit of Aggregation Does Not Correlate with Mutational Load

A possible mechanism explaining the advantage of collective infection is genetic complementation (sometimes referred to as multiplicity reactivation), whereby viral genomes carrying lethal or deleterious mutations regain infectivity and fitness in cells coinfected by other genomes that do not contain the same genetic defects [17, 18]. According to this hypothesis, a fraction of lethal mutations would be rescued in aggregates, increasing the number of viral genomes that effectively initiate the infection. Because this process should correlate with the population mutational load, to explore the role of genetic complementation, we subjected the virus to chemical mutagenesis by performing three serial transfers in the presence of the base analog 5-fluorouracil (5-FU), as detailed previously [19]. VSV-GFP and VSV-mCherry were mutagenized separately and then used to perform competition assays as above. The fluorescence signal was weaker and grew more slowly in 5-FU-treated viruses than in untreated viruses, consistent with an increased abundance of deleterious mutations. Yet aggregation had no significant effect on fitness, as determined by the fraction of GFP to total fluorescence at endpoint (34 hpi; 60.0% ± 3.4% in competitions with aggregated VSV-GFP versus monodisperse VSV-mCherry particles; 65.2% ± 2.0% using monodisperse VSV-GFP versus aggregated VSV-mCherry; t test: p = 0.261; Figure 3A). Furthermore, in mutagenized viruses, aggregation slowed down viral spread, reducing both the exponential growth rate (0.553 ± 0.001 versus 0.315 ± 0.012; t test: p < 0.001) and the maximal fluorescent area (58.1% ± 2.0% versus 20.0% ± 1.6%; t test: p < 0.001; Figure 3B). Therefore, increasing the mutational load reversed the fitness benefits of aggregation, contradicting the genetic complementation hypothesis.
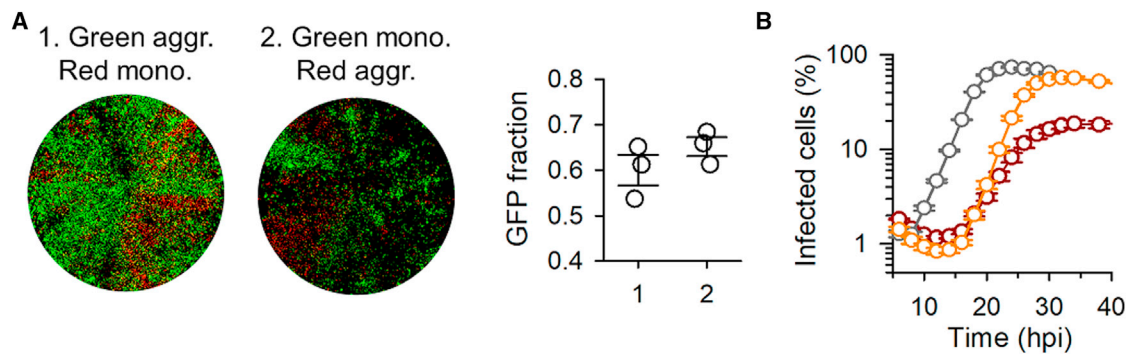
Figure 3. The Fitness Benefit of Aggregation Is Lost in Mutagenized Populations

(A) Whole-well fluorescence microscopy of MEFs inoculated with aggregated VSV-GFP and monodisperse VSV-mCherry particles (1) and with monodisperse VSV-GFP and aggregated VSV-mCherry particles (2). VSV-GFP and VSV-mCherry were mutagenized prior to competition assays using 5-FU. Images were taken at 34 hpi and correspond to one of the three replicate assays. The fraction of total fluorescent area occupied by GFP-positive cells is shown in the right graph for the three replicates. Error bars represent SEM.

(B) Growth curve of VSV in MEFs by real-time whole-well fluorescence microscopy. The percentage of fluorescent cells in the well is shown. Grey, non-mutagenized, monodisperse inoculum; orange, mutagenized, monodisperse inoculum; red: mutagenized, aggregated inoculum. Each data point is the average of three replicates. Error bars represent SEM.

The Benefits of Aggregation Correlate with Cell Permissivity to Infection

We set out to test whether our results were reproduced in baby hamster kidney fibroblasts (BHK-21), which are used routinely for VSV studies in part due to their high permissivity to VSV but which, as opposed to MEFs, are highly abnormal, tumoral cells. Competition assays, titrations at 4–6 hpi, and analysis of foci production showed that initiating the infection with saliva-aggregated particles provided a fitness advantage, although weaker than in MEFs (Figure S1). Titration of supernatants from BHK-21 cells inoculated at increasing cMOI values were also compatible with an Allee effect at the cellular level but less markedly than in MEFs (Figure S2). To examine such cell dependence in more detail, we used 4T1 mouse mammary gland tumor cells (epithelial), CT26 mouse colon cancer cells (fibroblasts), Neuro2a mouse neuroblastoma cells (neural stem-like cells), A549 human lung adenocarcinoma cells (alveolar epithelium), MRC5 human lung fibroblasts, and African green monkey Vero kidney epithelial cells. For this extended analysis, we focused only on competition assays with GFP and mCherry reporters and on titrations at 4–6 hpi. Initiating the infection with aggregates was selectively beneficial in MRC5, CT26, A549, and 4T1 in addition to MEFs and BHK-21, whereas it was detrimental in Vero and Neuro2a cells, as determined by the ratio of GFP to total fluorescence at endpoint (Figure S3; t tests: p < 0.001 in all cases). Hence, aggregation was most highly advantageous in the two non-tumoral cells lines tested (MEFs and MRC5). To measure cellular permissivity to VSV, we calculated the foci formation efficiency in each cell type, defined as the ratio of foci to viral particles present in a given inoculum (also termed specific infectivity), where viral particle concentration was determined by nanoparticle tracking analysis (Figure S4). The fitness benefit of aggregation, as indicated by competition assays, correlated inversely with foci formation efficiency among cells (Pearson correlation in log scale: r = −0.770; p = 0.025; Figure 4A), indicating that aggregation tended to be more beneficial in less permissive cells. Titration assays showed that, in most cells, the viral progeny derived from

monodisperse inocula was not detectable at 4 hpi, whereas aggregates tended to be slightly more productive, except in Neuro2a cells (Table S1). The effects of aggregation on viral titers were more easily quantified at 6 hpi and showed a significant increase in MEFs and MRC5 cells (t tests: p < 0.05) and a reduction in Neuro 2a, Vero, and 4T1 cells (p < 0.05; Table S1). Overall, aggregation accelerated progeny production at 6 hpi in less productive cells, as determined by the ratio of titers produced by aggregated and monodisperse inocula (r = −0.795; p = 0.018; Figures 4B and S5). Hence, again, aggregation tended to be more beneficial in difficult-to-infect cells.

Aggregation Is More Advantageous in Cells Displaying Stronger Innate Immune Antiviral Signaling

The ability of VSV to infect a given cell type depends, among other factors, on whether cells can mount a robust antiviral response. To explore the association between the fitness advantage of aggregation and innate immunity, we used a VSV variant that carries a deletion in methionine 51 of the matrix protein M (Δ51) [20]. Whereas the wild-type protein M inhibits host gene expression, this function is severely impaired in the Δ51 variant, allowing cells to express antiviral genes more strongly [20–22]. As a result, VSV-Δ51 is attenuated in normal cells, but not in cells with innate immunity defects, such as most tumor cells [20]. Therefore, by comparing the titer yield of wild-type VSV and VSV-Δ51, we can obtain information about the ability of a given cell type to signal an innate immunity response. We found that the wild-type/Δ51 titer ratio at 24 hpi correlated positively with the fitness benefit of aggregation, suggesting that initiating the infection in an aggregated manner increases the chances of the virus to overcome innate immunity (r = 0.722; p = 0.043; Figures 4C and 4D). To explore this further, we tested whether aggregation afforded a fitness benefit in cytokine-stimulated cells. For this, we first infected MEFs with VSV-Δ51 and filtered the supernatant through 50-nm size-exclusion columns to remove the virus and collect interferon and other cytokines. Then, we primed MEFs with
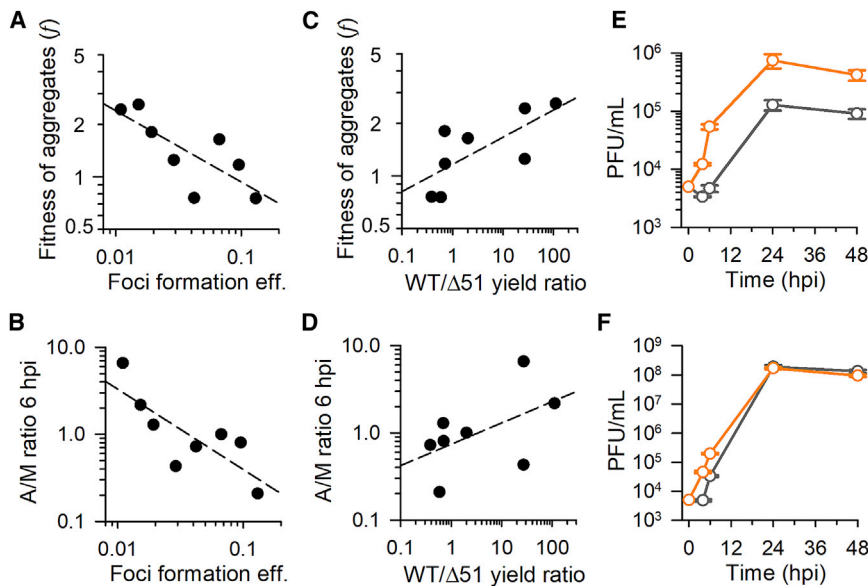
Figure 4. The Fitness Effects of Aggregation Depend on Cell Type and Innate Immunity

(A–D) Analysis of MEFs, MRC5, CT26, A549, 4T1, BHK-21, Vero, and Neuro2a cells. Each data point corresponds to one cell type (average of three measurements). Dashed lines indicate least-squares regressions.

(A and B) The foci formation efficiency (ratio of foci to viral particles in the inoculum) was used as an indicator of cell permissivity to infection. The particle concentration was determined by nano-particle tracking analysis (Figure S4).

(A and C) The fitness of aggregates was calculated as $f = P_G/P_R$, where P_G is the fraction of GFP to total fluorescence in competitions between aggregated VSV-GFP and monodisperse VSV-Cherry founders and P_R the GFP to total fluorescence ratio in competitions between monodisperse VSV-GFP and aggregated VSV-Cherry founders. Whole-well images used for inferring f are shown in Figure S3.

(B and D) The viral titers produced at 6 hpi by A and M inocula were determined by the plaque assay. The ratio of these two titers is shown. Titers for each M and A inocula are shown in Figure S5.

(C and D) The ratio of maximal titers reached by the wild-type (WT) and Δ51 variants was used as an indicator of the ability of a given cell type to mount an antiviral innate immune response.

(E and F) Growth curves produced by monodisperse (gray) and aggregated (orange) founders in MEFs primed with cytokines from a previous Δ51 infection (E) and in non-primed MEFs (F). Each data point is the average of three replicates. Error bars represent SEM.

Data are provided in Table S1.

this conditioned medium for 1 hr before adding the virus. In primed MEFs, viral spread was highly inefficient, resulting in a final titer reduction of more than two orders of magnitude compared to non-primed cells ($<10^6$ versus $>10^8$ PFU/mL; Figures 4E and 4F). Under these conditions, fast initial growth strongly determined viral yield, and infections founded by aggregates achieved an endpoint titer five-fold higher than those founded with monodisperse particles (t test: p = 0.006; Figure 4E), whereas in non-primed cells, final yields were similar (t test: p = 0.097; Figure 4F). Therefore, the fitness benefit of aggregation was exacerbated in cells displaying a strong antiviral response.

The Benefits of Aggregation Precede Cytokine-Mediated Innate Immunity in Non-primed Cells

The fitness benefits of aggregation occurred during the first infection cycle, but cytokine-mediated antiviral responses tend to be deployed later [23]. We therefore reasoned that the advantage of aggregation did not reside in blocking innate immunity but in producing a burst of progeny that could spread to other cells before the onset of antiviral responses. To test this, we measured expression levels of the interferon-stimulated gene Mx2 by RT-qPCR at 6 hpi in MEFs inoculated with aggregated versus monodisperse particles. In both cases, Mx2 expression was more than a thousand-fold lower than that of the housekeeping gene actin, consistent with the benefits of aggregation occurring before the innate immune response. Furthermore, Mx2 expression levels were higher in cells infected with aggregates than in those infected with monodisperse particles ($\log_{10}$ ratio of Mx2/actin mRNA levels: -3.926 ± 0.039 versus -4.316 ± 0.114; t test: p = 0.032). Hence, interferon-signaled immunity was not blocked in cells infected with viral aggregates but rather appeared to simply follow virus infection.

Faster Growth of Aggregates Also Occurs in the Absence of Saliva

Finally, we set out to explore whether the fitness advantage of aggregation could be driven by some component of the saliva promoting infectivity. In principle, this was unlikely because saliva-treated particles were diluted strongly prior to inoculation (>1,000-fold). Furthermore, this would not explain why aggregates outcompeted monodisperse particles in the same culture dish, except if the hypothetical proviral component was attached to virus aggregates and increased the permissivity of cells infected by aggregates, but not of other cells. To test whether aggregation increased fitness in the absence of saliva, we took advantage of the fact that aggregation occurs spontaneously at 37°C in high-titer preparations of gradient-purified virions [3]. Because this process is accompanied by significant virion degradation, we quantified the effect of degradation to establish our comparison for an equal infectious particle input. In competition assays between aggregated VSV-GFP and monodisperse VSV-mCherry, $43.9\% \pm 3.8\%$ of the total fluorescence signal corresponded to GFP at 24 hpi, whereas this fraction dropped to $33.4\% \pm 0.2\%$ when we competed monodisperse VSV-GFP against aggregated VSV-mCherry (t test: p = 0.049; Figure 5). Hence, initiating the infection with particles aggregated by this method also increased viral fitness, albeit the effect was clearly less marked than with saliva. We also performed titrations at 4–6 hpi. Aggregation produced a 4.2-fold increase in titer at 4 hpi (t test: p < 0.001) and an 8.6-fold increase at 6 hpi (p < 0.001) after correcting for particle degradation (Table 1).

1. Green aggr. Red mono.
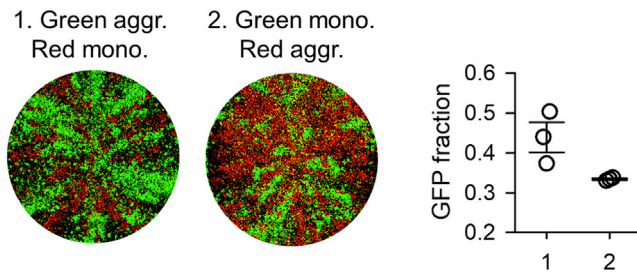
2. Green mono. Red aggr.

Figure 5. Fitness Effects of Spontaneous Viral Aggregation in the Absence of Saliva

Whole-well fluorescence microscopy images of cultures inoculated with aggregated VSV-GFP and monodisperse VSV-mCherry particles (1) and with monodisperse VSV-GFP and aggregated VSV-mCherry particles (2). Images were taken at 24 hpi and correspond to one of the three replicate assays performed. The fraction of total fluorescent area occupied by GFP-positive cells is shown in the right graph for the three replicates. Error bars: SEM.

Hence, the effect of aggregation on early viral proliferation also occurred in the absence of saliva. We note, however, that the benefits of aggregation with and without saliva are difficult to compare because of particle degradation and because the sizes of the aggregates might differ. At present, hence, we cannot formally discard the possibility that saliva might contain a proviral component that associates with viral aggregates.

DISCUSSION

Under the common perception that viruses propagate as individual virions, high cellular MOI values occur once intra-host viral densities have reached values that are sufficiently high to produce frequent coinfections by independent particles. Thus, under this conception, it is difficult to envisage how a virus could overcome Allee effects operating at the cellular level during the early stages of infection. In contrast, if viruses can propagate as collective infectious units, high cMOI values can be reached even in the very first infected cells and even if infections are initiated by a very small number of viral particles. As such, collective spread may help overcome Allee effects taking place during inter-host transmission, as well as during intra-host dissemination to new tissues and organs. The oral cavity is a preferred site of VSV replication and shedding in infected animals [24–26], and hence, the aggregating effect of saliva could have implications for the efficacy of virus transmission in nature.

A critical or strong Allee takes place when populations go extinct or fail to establish below a certain density threshold, whereas a weak or non-critical Allee effect takes place when fitness drops at low densities but is not low enough to trigger extinction [14]. Addressing this question in viruses is complicated by the fact that individuals (i.e., potentially infectious particles) are not counted directly. Although it is possible to use physical methods to enumerate viral particles, such as electron microscopy, nanoparticle tracking analysis, or tunable resistive pulse sensing, among others [27], a highly variable and often large fraction of particles is believed to be intrinsically non-infectious due to structural and/or genetic defects [28]. For this reason, viruses are typically enumerated using infectivity assays, such as the plaque or foci assay and/or related methods. How-

Table 1. Early Viral Progeny Production as Determined by Titration Assays (PFU/mL) in MEFs Inoculated with Purified, Monodisperse versus Aggregated Virions

	Monodisperse	Aggregated (Uncorrected)	Aggregated (Corrected for Degradation)
4 hpi	$(7.6 \pm 0.5) \times 10^3$	$(8.2 \pm 0.7) \times 10^3$	$(3.1 \pm 0.3) \times 10^4$
6 hpi	$(2.6 \pm 0.1) \times 10^5$	$(5.8 \pm 0.3) \times 10^5$	$(2.2 \pm 0.1) \times 10^6$

ever, this precludes detection of critical Allee effects, because population sizes are estimated based on methods that count units capable of establishing a productive infection. In VSV infecting BHK-21, it has been suggested that the PFU/particle ratio is close to 1.0 [29], meaning that most individual particles are capable of infecting cells efficiently and, hence, that no critical Allee effect could be operating. In contrast, here, we have estimated that this ratio is on the order of 0.1 for VSV in BHK-21 cells and as low as 0.01 in MEFs. We hence argue that the majority of viral particles fail to initiate infection in MEFs and other cell types despite containing no intrinsic structural or genetic defects, allowing for critical Allee effects. *In vivo*, viruses typically require a minimal dose for establishing infections, also suggesting critical Allee effects, but whether this barrier to infection operates at the cellular level or at other levels (organs and entire host) remains to be clarified.

In principle, genetic complementation offers a plausible mechanism for critical Allee effects in viruses, particularly in RNA viruses, which exhibit high mutation rates and hence high mutational loads [30]. However, the competitive advantage of aggregation was lost in our mutagenized viruses. Furthermore, aggregation reduced the overall growth of mutagenized populations. A possible explanation for these results is that genetic complementation allowed deleterious or lethal mutants present in aggregates to initiate infection but that these mutants interfered with fitter variants at one or several steps of the infection cycle, reducing their fitness. A possible way of producing this interference is by triggering host antiviral responses. This could contribute to explaining why populations founded by aggregates grew more poorly than those founded by monodisperse particles because, in the latter, these mutants would fail to replicate and hence may not trigger innate immunity efficiently.

The fitness benefit of initiating the infection with aggregates was cell type dependent. In the two non-tumoral cells examined (MEFs and MRC5), aggregation provided a clear fitness benefit as judged by plaque assays, whereas in tumoral cells, the effects were weaker and variable. Undoubtedly, the results obtained with MEFs and MRC5 cells are more likely to capture processes occurring in natural infections than those obtained with tumoral cells. In addition, the observed differences between tumoral and normal cells suggest candidate mechanisms for the Allee effect. Most tumoral cells exhibit innate immunity defects, rendering them more susceptible to infection than normal cells [20]. Even if the advantage of initiating cellular infection collectively preceded the onset of cytokine-mediated innate immunity, rapid diffusion of interferon in the medium might limit viral spread among neighbor cells [23, 31]. Concentrating the infection in fewer cells, each receiving a higher dose of particles, may allow the virus to stay ahead of such cellular innate immunity responses. It is also possible that the benefits of collective

infection are related to other, earlier barriers to infection. These could include interferon-independent antiviral mechanisms triggered by pathogen-associated molecular patterns in the first infected cells. Alternatively, collective infection might reduce the risk of stochastic loss of essential viral components during the very first stages of the cellular infection cycle. All VSV proteins are essential for infection but are expressed at different levels. Failure to produce sufficient levels of rate-limiting proteins, such as, for instance, the viral polymerase, could result in abortive infection, particularly in less active cells (here, non-tumoral cells). Entry of multiple particles to the same cell would reduce the risk of abortive infection because viral proteins produced by different infecting genomes would be shared, and hence, early expression defects could be compensated.

Although Allee effects have not been examined directly in viruses previously, there is some evidence suggesting that collective infectious units are fitter than individual particles. For example, in poliovirus, cells infected with vesicle-encapsulated virions exhibited higher viral RNA production than free virions [5]. Also, in infectious bursal disease virus, polyploid capsids showed greater infectivity than haploid capsids [32]. Interestingly, inoculation of individual cells with vaccinia virus particles using microfluidics revealed that the probability of establishing a successful infection increased logistically with the number of particles placed per cell, revealing cooperative interactions during the early stages of infection suggestive of an Allee effect [33]. However, because in these studies, per-capita viral proliferation rates were not determined, it was not possible to assess the net effect of collective infection on viral fitness. In future work, it would be interesting to evaluate whether our results apply to other viruses.

STAR★METHODS

Detailed methods are provided in the online version of this paper and include the following:

- KEY RESOURCES TABLE
- CONTACT FOR REAGENT AND RESOURCE SHARING
- EXPERIMENTAL MODEL AND SUBJECT DETAILS
  - Cell lines and culture
  - Virus
  - Saliva collection
- METHOD DETAILS
  - Viral titration
  - Viral aggregation in the presence of saliva
  - Gradient purification of virions
  - Aggregation of gradient-purified virions
  - Determination of foci formation efficiency
  - Quantitative analysis of foci
  - Automated real-time fluorescence microscopy
  - Chemical mutagenesis
  - Purification of cytokine-conditioned medium
  - RT-qPCR
- QUANTIFICATION AND STATISTICAL ANALYSIS

SUPPLEMENTAL INFORMATION

Supplemental Information includes five figures and one table and can be found with this article online at https://doi.org/10.1016/j.cub.2018.08.028.

AUTHOR CONTRIBUTIONS

I.A.-M. conducted the experiments, acquired data, contributed data analysis, and contributed manuscript preparation. R.S. designed research, contributed data analysis, and wrote the article.

DECLARATION OF INTERESTS

The authors declare no competing interests.

REFERENCES

1. Sanjuán, R. (2017). Collective infectious units in viruses. Trends Microbiol. 25, 402–412.

2. Altan-Bonnet, N. (2016). Extracellular vesicles are the Trojan horses of viral infection. Curr. Opin. Microbiol. 32, 77–81.

3. Cuevas, J.M., Durán-Moreno, M., and Sanjuán, R. (2017). Multi-virion infectious units arise from free viral particles in an enveloped virus. Nat. Microbiol. 2, 17078.

4. Aguilera, E.R., Erickson, A.K., Jesudhasan, P.R., Robinson, C.M., and Pfeiffer, J.K. (2017). Plaques formed by mutagenized viral populations have elevated coinfection frequencies. MBio 8, e02020-16.

5. Chen, Y.H., Du, W., Hagemeijer, M.C., Takvorian, P.M., Pau, C., Cali, A., Brantner, C.A., Stempinski, E.S., Connelly, P.S., Ma, H.C., et al. (2015). Phosphatidylserine vesicles enable efficient en bloc transmission of enteroviruses. Cell 160, 619–630.

6. Arantes, T.S., Rodrigues, R.A., Dos Santos Silva, L.K., Oliveira, G.P., de Souza, H.L., Khalil, J.Y., de Oliveira, D.B., Torres, A.A., da Silva, L.L., Colson, P., et al. (2016). The large Marseillevirus explores different entry pathways by forming giant infectious vesicles. J. Virol. 90, 5246–5255.

7. Slack, J., and Arif, B.M. (2007). The baculoviruses occlusion-derived virus: virion structure and function. Adv. Virus Res. 69, 99–165.

8. Pais-Correia, A.M., Sachse, M., Guadagnini, S., Robbiati, V., Lasserre, R., Gessain, A., Gout, O., Alcover, A., and Thoulouze, M.I. (2010). Biofilm-like extracellular viral assemblies mediate HTLV-1 cell-to-cell transmission at virological synapses. Nat. Med. 16, 83–89.

9. Murooka, T.T., Deruaz, M., Marangoni, F., Vrbanac, V.D., Seung, E., von Andrian, U.H., Tager, A.M., Luster, A.D., and Mempel, T.R. (2012). HIV-infected T cells are migratory vehicles for viral dissemination. Nature 490, 283–287.

10. Mothes, W., Sherer, N.M., Jin, J., and Zhong, P. (2010). Virus cell-to-cell transmission. J. Virol. 84, 8360–8368.

11. Erickson, A.K., Jesudhasan, P.R., Mayer, M.J., Narbad, A., Winter, S.E., and Pfeiffer, J.K. (2018). Bacteria facilitate enteric virus co-infection of mammalian cells and promote genetic recombination. Cell Host Microbe 23, 77–88.e5.

12. Anderson, D.J., and Le Grand, R. (2014). Cell-associated HIV mucosal transmission: the neglected pathway. J. Infect. Dis. 210 (Suppl 3), S606–S608.

13. Taylor, C.M., and Hastings, A. (2005). Allee effects in biological invasions. Ecol. Lett. 8, 895–908.

14. Kramer, A.M., Dennis, B., Liebhold, A.M., and Drake, J.M. (2009). The evidence for Allee effects. Popul. Ecol. 51, 341.

15. Shapiro-Ilan, D.I., Lewis, E.E., and Schliekelman, P. (2014). Aggregative group behavior in insect parasitic nematode dispersal. Int. J. Parasitol. *44*, 49–54.

16. Kaul, R.B., Kramer, A.M., Dobbs, F.C., and Drake, J.M. (2016). Experimental demonstration of an Allee effect in microbial populations. Biol. Lett. *12*, 20160070.

17. Sanjuán, R. (2018). Collective properties of viral infectivity. Curr. Opin. Virol. *33*, 1–6.

18. Andino, R., and Domingo, E. (2015). Viral quasispecies. Virology *479-480*, 46–51.

19. Sanjuán, R., Cuevas, J.M., Furió, V., Holmes, E.C., and Moya, A. (2007). Selection for robustness in mutagenized RNA viruses. PLoS Genet. *3*, e93.

20. Stojdl, D.F., Lichty, B.D., tenOever, B.R., Paterson, J.M., Power, A.T., Knowles, S., Marius, R., Reynard, J., Poliquin, L., Atkins, H., et al. (2003). VSV strains with defects in their ability to shutdown innate immunity are potent systemic anti-cancer agents. Cancer Cell *4*, 263–275.

21. Rajani, K.R., Pettit Kneller, E.L., McKenzie, M.O., Horita, D.A., Chou, J.W., and Lyles, D.S. (2012). Complexes of vesicular stomatitis virus matrix protein with host Rae1 and Nup98 involved in inhibition of host transcription. PLoS Pathog. *8*, e1002929.

22. Quan, B., Seo, H.S., Blobel, G., and Ren, Y. (2014). Vesiculoviral matrix (M) protein occupies nucleic acid binding site at nucleoporin pair (Rae1 ● Nup98). Proc. Natl. Acad. Sci. USA *111*, 9127–9132.

23. Voigt, E.A., Swick, A., and Yin, J. (2016). Rapid induction and persistence of paracrine-induced cellular antiviral states arrest viral infection spread in A549 cells. Virology *496*, 59–66.

24. Scherer, C.F., O'Donnell, V., Golde, W.T., Gregg, D., Estes, D.M., and Rodriguez, L.L. (2007). Vesicular stomatitis New Jersey virus (VSNJV) infects keratinocytes and is restricted to lesion sites and local lymph nodes in the bovine, a natural host. Vet. Res. *38*, 375–390.

25. Smith, P.F., Howerth, E.W., Carter, D., Gray, E.W., Noblet, R., Berghaus, R.D., Stallknecht, D.E., and Mead, D.G. (2012). Host predilection and transmissibility of vesicular stomatitis New Jersey virus strains in domestic cattle (*Bos taurus*) and swine (*Sus scrofa*). BMC Vet. Res. *8*, 183–188.

26. Smith, P.F., Howerth, E.W., Carter, D., Gray, E.W., Noblet, R., and Mead, D.G. (2009). Mechanical transmission of vesicular stomatitis New Jersey virus by *Simulium vittatum* (Diptera: *Simuliidae*) to domestic swine (*Sus scrofa*). J. Med. Entomol. *46*, 1537–1540.

27. Heider, S., and Metzner, C. (2014). Quantitative real-time single particle analysis of virions. Virology *462-463*, 199–206.

28. Klasse, P.J. (2015). Molecular determinants of the ratio of inert to infectious virus particles. Prog. Mol. Biol. Transl. Sci. *129*, 285–326.

29. Akpinar, F., and Yin, J. (2015). Characterization of vesicular stomatitis virus populations by tunable resistive pulse sensing. J. Virol. Methods *218*, 71–76.

30. Sanjuán, R., and Domingo-Calap, P. (2016). Mechanisms of viral mutation. Cell. Mol. Life Sci. *73*, 4433–4448.

31. Howat, T.J., Barreca, C., O'Hare, P., Gog, J.R., and Grenfell, B.T. (2006). Modelling dynamics of the type I interferon response to in vitro viral infection. J. R. Soc. Interface *3*, 699–709.

32. Luque, D., Rivas, G., Alfonso, C., Carrascosa, J.L., Rodríguez, J.F., and Castón, J.R. (2009). Infectious bursal disease virus is an icosahedral polyploid dsRNA virus. Proc. Natl. Acad. Sci. USA *106*, 2148–2152.

33. Stiefel, P., Schmidt, F.I., Dörig, P., Behr, P., Zambelli, T., Vorholt, J.A., and Mercer, J. (2012). Cooperative vaccinia infection demonstrated at the single-cell level using FluidFM. Nano Lett. *12*, 4219–4227.

34. Lawson, N.D., Stillman, E.A., Whitt, M.A., and Rose, J.K. (1995). Recombinant vesicular stomatitis viruses from DNA. Proc. Natl. Acad. Sci. USA *92*, 4477–4481.

35. Palmero, I., and Serrano, M. (2001). Induction of senescence by oncogenic Ras. Methods Enzymol. *333*, 247–256.

STAR★METHODS

KEY RESOURCES TABLE

REAGENT or RESOURCE	SOURCE	IDENTIFIER
Bacterial and Virus Strains		
VSV	Dr. J.K. Rose (Yale University School of Medicine) [34]	N/A
VSV-Δ51	Dr. J.C Bell (Ottawa University) [20]	N/A
Biological Samples		
Human Saliva	This paper and [3]	Anonymous donor
Chemicals, Peptides, and Recombinant Proteins		
5-Fluorouracil (5-FU)	Sigma-Aldrich	Cat# F6627
DAPI	Roche	Cat# 10236276001
Optiprep	Sigma-Aldrich	Cat# D1556
TRI Reagent Solution	Invitrogen	Cat# AM9738
SuperScript IV Reverse Transcriptase	Invitrogen	Cat# 18090050
2X Brilliant III Ultra-Fast SYBR Green QPCR Master Mix	Agilent	Cat# 600882
Experimental Models: Cell Lines		
Mouse: MEF (C57BL/6)	Dr. C. Rivas (Universidad de Santiago de Compostela)	N/A
Hamster: BHK-21	ATCC	ATCC Cat# CCL-10; RRID: CVCL_1915
Mouse: CT26	ATCC	ATCC Cat# CRL-2639; RRID: CVCL_7255
Mouse: 4T1	ATCC	ATCC Cat# CRL-2539; RRID: CVCL_0125
Cercopithecus aethiops: Vero	ATCC	ATCC Cat# CCL-81; RRID: CVCL_0059
Human: MRC-5	ATCC	ATCC Cat# CCL-171; RRID: CVCL_0440
Mouse: Neuro-2a	ATCC	ATCC Cat# CCL-131; RRID: CVCL_0470
Human: A549	ATCC	ATCC Cat# CCL-185; RRID: CVCL_0023
Oligonucleotides		
Primer: mouse Mx2 mRNA Reverse (RT): TGGAGTCGGATTGACATCTCTG	This paper	N/A
Primer: mouse β-actin mRNA Reverse (RT): CAGAGGCATACAGGGACAGC	This paper	N/A
Primer: mouse Mx2 mRNA Forward: ACACGGTCACTGAAATTGTACG	This paper	N/A
Primer: mouse Mx2 mRNA Reverse: TCATCTTTTCACGGTTGGCTT	This paper	N/A
Primer: mouse β-actin mRNA Forward: CTGGCACCACACCTTCTACA	This paper	N/A
Primer: mouse β-actin mRNA Reverse: TCATCTTTTCACGGTTGGCTT	This paper	N/A
Software and Algorithms		
Fiji (ImageJ)	NIH / public domain	https://fiji.sc/
R version 3.x	R Project	https://www.R-project.org/

CONTACT FOR REAGENT AND RESOURCE SHARING

Further information and requests for resources and reagents should be directed to and will be fulfilled by the Lead Contact, Rafael Sanjuán (rafael.sanjuan@uv.es).

EXPERIMENTAL MODEL AND SUBJECT DETAILS

Cell lines and culture

MEFs derived from C57BL/6 mice embryos were isolated in previous work by Dr. Carmen Rivas (Universidad de Santiago de Compostela, Spain) following standard procedures [35]. No information about the gender or exact age of the source animals was available. BHK-21 (CCL-10), A549 (CCL-185), 4T1 (CRL-2539), CT26 (CRL-2639), MRC5 (CCL-171), Neuro2a (CCL-131) and Vero (CCL-81) cells were obtained from the American Type Culture Collection (ATCC, reference number indicated in parentheses) and cultivated from low-passage stocks (typically below passage 10) for no more than 20 additional cell doublings. All cell lines were cultured in Dulbecco's modified Eagle's medium (DMEM) supplemented with 10% fetal bovine serum (FBS) at 37°C in a 5% CO_2 humidified incubator and tested mycoplasma-negative by PCR.

Virus

VSV was recovered from a cDNA clone originally created by Lawson et al. [34] and kindly provided by Dr. Valery Z. Grdzelishvili (University of North Carolina). Two variants of this clone were used with the GFP or mCherry gene cloned at the intergenic region between the G and L genes.

Saliva collection

Human saliva was provided with informed consent after seeking approval from the Ethics Committee of the Universitat de València. Saliva was filtered through a 0.45 μm cellulose filter to remove bacteria and debris, aliquoted, and stored at –70°C until use.

METHOD DETAILS

Viral titration

Confluent BHK-21 monolayers were used for virus titrations. The monolayers were inoculated with 200 μL of diluted viral suspensions for 45 min under standard culturing conditions (37°C, 5% CO_2) and then overlaid with DMEM supplemented with 2% FBS and 0.5% or 0.6% agar. After 20-24 h, cells were fixed with 10% formaldehyde, stained with 2% crystal violet in 10% formaldehyde, and plaques were counted.

Viral aggregation in the presence of saliva

The efficacy of saliva to produce viral aggregates varies among donors [3]. All human saliva used in this work was provided by a unique female volunteer who showed the strongest aggregating effects in our previous work [3]. A virus stock (ca. 10^9 PFU/mL) was diluted 1:10 in saliva, incubated at 37°C for 1 h, and diluted conveniently to infect cells (ca. 1000-fold).

Gradient purification of virions

Purified VSV-GFP and VSV-mCherry stocks were prepared by inoculating eight BHK-21 confluent T175 flasks at an MOI of 0.1 PFU/cell and collecting supernatants upon appearance of the first obvious cytopathic effects (ca. 14 hpi). Large cellular debris was removed by spinning (780 g, 5 min) and filtering (0.22 μm) supernatants. Virions were then pelleted at 30,000 g, 4°C, and 1.5 h in a Sorvall LYNX 6000 high-speed centrifuge with an A27-8 × 50 fixed-angle rotor. The virus pellet was resuspended in 2 mL 100mM NaCl, 0.5 mM EDTA.Na$_2$·2H$_2$O, 50mM Tris-HCl buffer (pH 7.4), laid on a iodixanol (Optiprep, Sigma) gradient in Nalgene polycarbonate oak ridge tubes, and centrifuged at 80,000 g, 4°C, 4.5 h. Approximately 700 μL of a whitish band generated at mid-gradient were collected, aliquoted and stored at –70°C.

Aggregation of gradient-purified virions

Gradient-purified stocks undergo spontaneous aggregation upon incubation at 37°C, but not at room temperature [3]. In high-titer purified stocks, a 30 min incubation produced frequent dual GFP/mCherry infection foci. However, this was accompanied by virion degradation. To correct for the degradation effect, we performed a calibration experiment in which we diluted the purified virions to 10^5 PFU/mL in the same buffer used for gradient purification. Under these conditions, aggregation became negligible because virion-virion contacts were highly unlikely, as shown by the fact that we saw no mixed GFP/mCherry foci. Hence, any change in titer was due to degradation. In this calibration experiment, after 30 min at 37°C the viral titer decayed by 3.8 ± 0.3 fold. Hence, we used this ratio as a correction factor to account for degradation, allowing us to compare the fitness of monodisperse and aggregated viruses for an equal infectious particle input.

Determination of foci formation efficiency

Gradient-purified virions were used for nanoparticle tracking analysis, which is based on video tracking of the light scattering produced by individual nanoparticles to measure their Brownian motion, obtain their diffusion coefficient, and infer their hydrodynamic diameter using Stokes-Einstein equation. Purified virions were loaded into a NanoSight NS300 equipment (Malvern) with the aid of a syringe pump to increase particle flow through the chamber, and analyzed by built-in software using default parameters. The size and

concentration of virions was inferred by counting particles in five video captures of 10 s each. Then, we performed plaque assays by inoculating monolayers of each cell line with known numbers of particles and counted the number of foci produced to determine the foci formation efficiency (foci to particle ratio).

Quantitative analysis of foci

Confluent cell monolayers were inoculated with a mix of VSV-GFP/VSV-mCherry containing aggregated or monodisperse viral particles for microscopic examination of short-term viral spread. Cells were fixed at different post-inoculation times with 4% paraformaldehyde, stored overnight at 4°C, rinsed with PBS 1X, stained with DAPI (Roche) and preserved in phosphate buffer with 0.05% azide until image acquisition. Multichannel fluorescence imaging of representative areas of the infected monolayers was performed on an IN Cell Analyzer 2000 (GE Healthcare). Filter channels used for imaging were FITC 490/20 nm excitation, 525/36 nm emission for GFP fluorescence; Texas Red 579/34 nm excitation, 624/40 nm emission for mCherry fluorescence, and DAPI 350/50 nm excitation, 455/50 nm emission for DAPI staining fluorescence with an exposure time of 400, 800 and 100 ms, respectively. Acquired images were visualized with Fiji (ImageJ) and the number of cells per infection foci was determined by manual counting, since high cell confluence extremely complicate an automated cell discrimination, especially in BHK-21 cells.

Automated real-time fluorescence microscopy

Imaging was performed in an IncuCyte S3 Live-Cell Analysis System (Essen BioScience) housed inside a humidified tissue culture incubator at 37°C and 5% CO_2. Images were acquired using phase contrast, green (300-ms exposure) and red (400-ms exposure) channels in the IncuCyte S3 platform with a 4X objective in triplicate. Representative images of various time points and experimental conditions were selected and used as a reference to define image analysis masks for each acquisition channel. Images were segmented by defining a fluorescence intensity threshold after applying a background correction using the Top-Hat method. When needed, masks were fine-tuned by setting maximum and minimum object areas and eccentricity values. To infer growth parameters we used a logistic growth model of the form $P_t = P_M/(1 + e^{c-rt})$, where t is the infection time, P_t is the percent of virus-positive cells (% confluence), P_M is the maximum P_t value, r is the exponential growth rate, and c sets the initial conditions. Half times were calculated as $t_{1/2} = c/r$. The model was fit to the data by non-linear least-squares regression. In competition, assays the fraction of the total fluorescent area, i.e., GFP/(GFP+mCherry), was determined at the time point yielding maximal total fluorescence (i.e., at the growth curve plateau). The fitness of populations derived from aggregated relative to monodisperse founders was calculated as $f = P_G/P_R$, where P_G is the fraction of GFP/total fluorescence in competitions between aggregated VSV-GFP and monodisperse VSV-Cherry founders, and P_R the GFP/total fluorescence in competitions between monodisperse VSV-GFP and aggregated VSV-Cherry founders.

Chemical mutagenesis

VSV-GFP and VSV-mCherry were subjected separately to three serial transfers in BHK-21 cells in the presence of 5-FU 40 ug/mL. For each passage, confluent cell monolayers were pre-treated with 5-FU for 6 h, inoculated with the virus ($D = 0.1$ PFU/cell) and incubated for 24 h in standard infection medium supplemented with 5-FU. After each transfer, supernatants were collected and titrated by the plaque assay. 5-FU was cleared from transfer-3 supernatants by pelleting the virus at 30,000 g for 1.5 h and resuspending the pellet in medium not containing 5-FU. Next, a one-step amplification was carried out to increase the viral titer, since saliva-driven aggregation is titer-dependent. This amplification step was done by inoculating BHK-21 monolayers at high density ($D = 10$ PFU/cell) and collecting the supernatant at 8 hpi. A high viral density inoculum was used to favor the maintenance of deleterious mutants produced during the mutagenesis transfers. To reach a titer similar to those of non-mutagenized stocks (10^9 PFU/mL), we finally concentrated the viruses tenfold by centrifugation at 30,000 g for 1.5 h. Saliva-driven aggregation was verified by mixing VSV-GFP and VSV-mCherry mutagenized stocks, incubating the mix in saliva (37°C, 1 h), and enumerating doubly fluorescent foci in standard plaque assays.

Purification of cytokine-conditioned medium

Cytokine-containing conditioned medium was obtained by infecting a confluent MEF monolayer with VSV-Δ51 mutant at ($D = 10$ PFU/cell) and collecting the infection medium approximately at 24 hpi. Cell debris was removed from the crude infection medium by centrifugation at 5000 g for 10 min, and the supernatant was cleared of viruses and other small particles using a 0.05 μm cellulose filter (MF-Millipore; VMWP02500). The resulting purified medium was then aliquoted, stored at –70°C, and checked for the absence of viruses by plaque assays of undiluted aliquots in BHK-21 cells.

RT-qPCR

Confluent MEF monolayers cultured in 6-well plates and inoculated ($D = 0.1$ PFU/cell) with equal-virion, aggregated/non-aggregated VSV-GFP suspensions were used for total RNA isolation using the acid guanidinium-thiocyanate-phenol-chloroform method (TRI Reagent Solution, Invitrogen), following manufacturer's instructions. Infected monolayers were overlaid with DMEM supplemented with 10% FBS after 45 min of virus incubation under standard culture conditions (37°C, 5% CO_2). At 6 hpi, the culture medium was removed and RNA was isolated. Output concentrations for all RNA samples were adjusted to 150 ng/μL, and 3 μL were added to reverse transcription (RT) reactions carried out with gene-specific primers for either mouse Mx2 mRNA (5′tggagtcggattgacatctctg) or the β-actin mRNA (5′cagaggcatacagggacagc), and SuperScript IV Reverse Transcriptase (Invitrogen). RT reactions were performed at 55°C, following manufacturer's instructions. The linear range of detection for the RT reaction was determined by serial

dilutions of extracted mRNAs. The qPCR was performed with primers for mouse Mx2 mRNA (5′acacggtcactgaaattgtacg, 5′tcatcttttcacggttggctt) or actin mRNA (5′ctggcaccacaccttctaca, 5′tcatcttttcacggttggctt) using the 2X Brilliant III Ultra-Fast SYBR Green QPCR Master Mix (Agilent) on an AriaMx machine (Agilent). The absence of contaminating DNA, primer-dimers and multiple amplicons in the reactions were tested by melting curve analysis and including no-RT and no-template controls. The following thermal profile was used for amplification: 95°C for 3 min, and 40 cycles of 95°C for 15 s and 60°C for 20 s.

QUANTIFICATION AND STATISTICAL ANALYSIS

All virus infections were conducted in triplicates and all measurements are reported as mean ± SEM. Statistical analyses were performed using SPSS software (IBM Analytics), and are indicated in the main text and SI figure legends. Model fitting explained in Methods Details was carried out by non-linear least-squares regression using the nls function implemented in R package (http://www.r-project.org) and model parameters were calculated for each replicate.